Investigating the effects of overlap and event durations on neural responses

Master Thesis

12. November 2022

Martin Geiger

3560767

University of Stuttgart

Institute of Sport and Movement Science

Supervisor: Prof. Dr. Nadja Schott

ABSTRACT

Event-related potentials (ERPs) provide an excellent temporal resolution to isolate neurocognitive processes. Neural responses intermingled in the electroencephalogram (EEG) must be distinguished to study the dynamics of sensory encoding, decision-making, and motor action that drive human behaviour. Two data-analytic challenges complicate the accurate estimation of ERPs: 1) Overlap of neural responses due to close temporal proximity of adjacent events. 2) Varying event durations, e.g. due to natural variation in response time (RT) or experimentally varying stimulus durations. In this study, I carried out an active visual oddball experiment and analysed the effects of overlap and varying event durations on neural responses. The analysis included the comparison of ERP estimates obtained from three regression-based models. Overlap correction with the deconvolution model revealed significant effects of overlap when compared to the traditional ERP averaging approach. Adding RT as a predictor modelled via spline regression disclosed that its natural variation over trials had a nonlinear effect on ERP estimates. Furthermore, modelling overlap and RT in one generalised additive model (GAM) simultaneously resulted in a significantly smaller difference between neural responses related to the processing of experimental conditions. A lack of consistency in the results obtained here with those of a previous study, which the experimental paradigm was adapted from, requires further analysis. The current study shows that overlap correction is crucial to disentangle stimulus- and response-locked neural responses. Overlap and varying event durations may lead to biased estimates and false inferences about brain dynamics if they are not controlled for. This highlights the importance of implementing sophisticated data-analytic methods for analysing EEG data recorded during complex experimental paradigms and naturalistic situations to achieve sensible ERP estimates.

TABLE OF CONTENTS

1 INTRODUCTION

As we move about this world, we continually extract information from our environment using our sensory organs. We then filter what is relevant and process it within our nervous system. Finally, we act upon the brain's decisions through fine-tuned movement actuated via the musculoskeletal system. These processes are remarkably complex and require sophisticated data-analytic methods that can take into account that different cognitive processes are carried out in parallel and that the duration to complete them is often variable.

The electroencephalogram (EEG) is one of the most popular methods to study neural dynamics and drives our understanding of how the human brain achieves such complex tasks. EEG is a record of the time course of extracellular field potentials generated by the synchronous, cooperative action of neuron populations. The neurophysiological basis of EEG is rooted in potential differences across the postsynaptic membrane. The binding of neurotransmitters to receptors results in the influx and efflux of cations (K^+, Na^+, Ca^{2+}) and anions (Cl^-). These ion currents along the cell membrane of cortical pyramidal neurons create postsynaptic potentials (PSPs) that result in small electric fields similar to dipoles (Figure 1). The sum of a large number of dipoles generated by synchronized PSPs in parallel orientation propagates to the EEG electrodes on the scalp almost at the speed of light (Blinowska & Durka, 2006; Luck, 2014). The EEG is, therefore, a direct and instantaneous measure of neural activity on a millisecond time scale, which sets it apart from other non-invasive brain imaging techniques to study neural dynamics (Luck, 2014).

Spontaneous EEG describes the brain-electric activity that is independent of stimuli. In contrast, event-related potentials (ERPs) are changes in spontaneous EEG evoked by external or internal stimuli (Blinowska & Durka, 2006). ERPs, therefore, enable us to isolate neurocognitive processes related to stimuli, responses, and other events with excellent temporal resolution (Kappenman et al., 2021a).

The domain focused on the measurement and interpretation of the EEG has two assumptions: 1) Measurements of electrical brain activity represent the linear sum of all sensory, cognitive, and motor processes that took place around the time point of sampling.

2) The brain is a linear time-invariant (LTI) system; therefore, neural responses related to the processing of events are independent of the time interval between their occurrences (Ehinger & Dimigen, 2019; Smith & Kutas, 2015b).

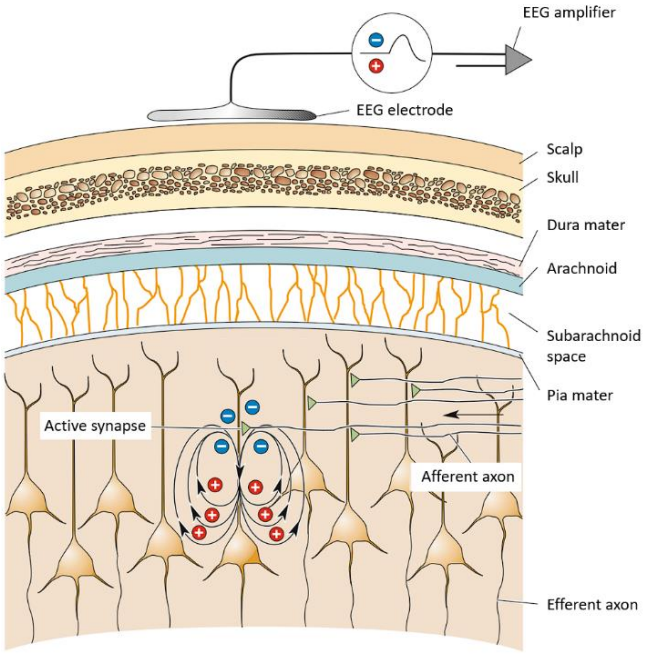

Figure 1. Postsynaptic potentials (PSPs) result in small electric fields measured as EEG signals on the scalp. Changes in the membrane potential along a cortical pyramidal neuron result in oppositely charged extracellular space along the neuron, creating a dipole. The sum of these electric fields created by the synchronous activity of a large number of neurons constitutes the EEG signal measured on the scalp. Adapted from *Neurowissenschaften* (p. 698) by Bear et al., 2018, Berlin Heidelberg: Springer, Copyright 2018 by Springer-Verlag.

1.1 ERP Averaging

EEG measurements suffer from a low signal-to-noise ratio (SNR). Therefore, the neural responses related to specific events (signal) need to be isolated from diverse non-brain artefacts (noise) to interpret recorded EEG data. The traditional approach to improve the SNR is ERP averaging. This method has been applied successfully in numerous EEG studies (Smith & Kutas, 2015a).

For ERP averaging, the continuous EEG data are first epoched by splitting them into equal-sized fragments time-locked to an event. Each epoch corresponds to one occurrence of the event of interest, usually one experimental trial. Afterwards, the point-by-point average of aligned epochs is calculated (Smith & Kutas, 2015a).

Mathematically, an ERP is estimated with the ordinary equation for computing the mean:

$$\frac{1}{n}\sum_{i=1}^{n} y_i = \beta \quad (1)$$

To estimate β, the value of an ERP at a single electrode and latency, the mean of all EEG data points y over epochs i is calculated. This is repeated for each latency in the epochs and all electrodes. The obtained β values are then concatenated into vectors for all electrodes, plotted and analysed as ERP estimates (Smith & Kutas, 2015a).

The rationale for ERP averaging is based on the assumption introduced above that ERPs are constant for different trials of the same event. At the same time, the noise is different on every trial. As a result, noise cancels out when averaging many trials while the part of the EEG signal that is present on every trial, the ERP, remains (Smith & Kutas, 2015a).

ERP averaging allows for gaining insight into neural processing dynamics with a millisecond-level resolution. ERP averaging, however, has several disadvantages. Experimental protocols are restricted to a small number of stimulus categories. This approach requires thoroughly controlled stimuli to hold all other cognitive processes constant. Moreover, events need adequate temporal spacing for optimal results (Smith & Kutas, 2015a).

1.2 TWO CHALLENGES

These requirements for the ERP averaging approach severely constrain the experimental design of EEG studies. Two obstacles arise for the analysis of EEG data recorded during less controlled experiments.

1.2.1 Overlap

Presentation of stimuli with short inter-stimulus intervals (ISIs) provides practical benefits such as collecting more data within a shorter time (Smith & Kutas, 2015b) and studying priming and habituation effects of successive stimuli (Woldorff, 1993).

Often tasks require fast-paced responses to stimuli. This allows, amongst others, to study cognitive control processes such as response inhibition (Huster et al., 2013),

dynamics of error processing in motor behaviour (Völker et al., 2018), and neural correlates of decision-making (Twomey et al., 2015).

There is also a growing interest in analysing brain activity during naturalistic situations. These include attentional processing under increased motor and environmental demands (Liebherr et al., 2021) and mobile brain/body imaging during active motor behaviour (Gramann et al., 2014).

The short time intervals between different events in studies like these constitute a major data-analytic challenge. Consider the very common two-choice oddball paradigm that is defined by three key characteristics: 1) A sequence of stimuli that each belongs to one of two classes is presented to a subject. 2) Occurrence of the stimuli assigned to one class is less frequent (targets) than of those assigned to the other class (distractors). 3) The subject's task is to categorise each stimulus into one of the two classes (Sellers et al., 2012). The time between the presentation of a stimulus and the subsequent behavioural response for categorisation is defined as response time (RT) (Horváth et al., 2018).

During the oddball task, RTs typically range from 300 to 500 ms (Kappenman et al., 2021b). However, ERPs frequently persist up to or even exceed a second before the signal returns to baseline (Blinowska & Durka, 2006; Dimigen & Ehinger, 2021; Smith & Kutas, 2015b). Therefore, neural activity related to stimulus onsets and the subsequent manual responses affects a single EEG sample - they overlap (Figure 2).

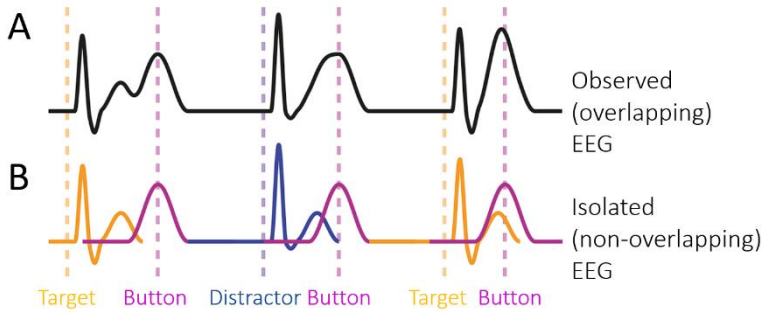

Figure 2. Illustration of measured EEG data obtained from overlapping neural responses. (A) The observed EEG represents the linear sum of (B) neural responses to stimulus onsets (target and distractor) and manual responses (button) that overlap due to the temporal proximity of the events they are evoked by. Adapted from "Unfold: an integrated toolbox for overlap correction, nonlinear modelling, and regression-based EEG analysis" by B. V. Ehinger and O. Dimigen, 2019, PeerJ, 7, e7838. CC-BY 4.0.

The main processing stages of the oddball task include sensory encoding, decision formation, and motor execution (Kelly & O'Connell, 2015; Twomey et al., 2015). With the traditional ERP averaging approach, it is impossible to determine which portion of the overlapping EEG data is attributable to each process (Ehinger & Dimigen, 2019; Smith & Kutas, 2015b). However, using such simple sensory-motor tasks that allow precise control over sensory input and quantification of motor output (Gold & Shadlen, 2007) may improve our understanding of how these core processes can be disentangled. This will drive studies of more complex experimental paradigms and naturalistic situations.

1.2.2 Varying event durations

Another challenge for accurately estimating ERP waveforms is the influence of varying event durations. A magnetoencephalography (MEG) study showed that experimental variation of stimulus duration affects face recognition and cortical activation (Tanskanen et al., 2007). The impact of fixation duration on the learning process has been revealed in an eye-tracking experiment (Negi & Mitra, 2020).

RT naturally varies between trials and subjects in tasks that require motor responses. This manifests in the variability of response latency relative to stimulus onsets. Kutas et al. (1977) showed that adjustment for trial-by-trial variability in latency (also known as latency jitter) resulted in larger averaged P300 amplitudes. Latency jitter, rather than merely lowering its amplitude, also increases the averaged component's latency (Figure 3) (Dimigen & Ehinger, 2021; Rossion & Jacques, 2008). This smearing of the estimated waveform across time can obscure amplitude differences between conditions and lead to misinterpretation of condition effects (Murray et al., 2019).

Furthermore, in the oddball experiment, RTs are typically shorter for distractor stimuli than target stimuli (see Results, Figure 8). Therefore, motor responses overlap on average 70 ms earlier in the distractor condition. If not considered, this difference in mean RT between conditions will confound ERP estimates and lead to inadequate inferences about underlying neural processes.

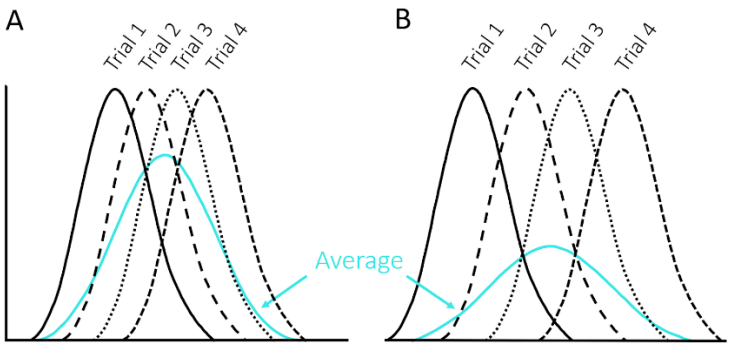

Figure 3. Effect of inter-trial variability in latency on averaged waveforms. Illustrated are four single-trial waveforms along with their average. (A) Low latency variability results in a smaller effect on the average waveform than (B) high latency jitter. In (B), the peak amplitude is smaller, and the temporal range of the average waveform is greater. Adapted from "Compensation of trial-to-trial latency jitter reveals the parietal retrieval success effect to be both variable and thresholded in older adults" by J.G. Murray, G. Ouyang and D.I. Donaldson, 2019, Frontiers in Aging Neuroscience, 11:179. CC-BY.

Late components are generally more affected by latency jitter than earlier components. Additionally, the latency of the P300 component depends on the time needed for stimulus categorisation, which is especially variable between trials. P300 latency and amplitude are thus highly affected by the inter-trial variability of RT (Luck, 2014). For this reason, it may be especially important to control for natural RT variability when analysing the results of an oddball task, as the P300 component is the part of the signal that is usually evaluated.

Because varying event durations affect neural processing, and since there can be differences between conditions, as for RT, it is crucial to prevent biased ERP estimates by implementing analysis approaches that can account for them. Creating "ERP images" from epoched data facilitates the investigation of how continuous covariates like RT affect the ERP (Jung et al., 2001). However, only the effect of one covariate can be visualised per image, and confounding cannot be controlled (Smith & Kutas, 2015a).

1.3 Regression-based EEG analyses

Regression-based approaches have gained increasing popularity for the analysis of EEG data. The regression-ERP framework allows for more flexible experimental designs with categorical and continuous covariates. It can control for linear and nonlinear confounds on ERP waveforms and can be applied to disentangle overlapping neural responses to

adjacent events (Dimigen & Ehinger, 2021; Ehinger & Dimigen, 2019; Smith & Kutas, 2015a).

In the following, I will explain the regression-based approaches of mass-univariate linear modelling, linear deconvolution modelling for overlap correction, and spline regression alongside considerations of which experimental designs are appropriate. I will first delineate the conceptual and mathematical basics in regression terminology to facilitate comprehension of matrix notation later on.

1.3.1 Least Squares Regression

Assume we want to calculate the value of an ERP at a single electrode and latency, e.g. 100 ms after the onset of a target stimulus t. A measured data point *y* on trial *i* comprises the evoked brain activity we intend to estimate, the β_t value, and noise. Therefore, one data point of a target trial would be represented by

$$y_i = \beta_t + noise_i \tag{2}$$

All data points measured at that electrode with equal latency relative to the time-locking event (+100 ms) are then averaged over the epochs. Formally, the least squares principle postulates to estimate β as the value that results in the smallest possible squared noise:

$$squared\ noise = \sum_{i=1}^{n} (noise_i)^2 = \sum_{i=1}^{n} (y_i - \beta)^2 \tag{3}$$

This is mathematically equal, as proven by Smith and Kutas (2015a), to the ordinary equation (1) for computing the mean. The calculation is repeated for each latency in the epochs and all electrodes. Obtained β values are then concatenated into vectors for all electrodes, plotted and analysed as ERP estimates.

Since these ERP estimates are obtained by regression, they are commonly referred to as regression-ERPs (rERPs). However, this nomenclature relates only to the mathematical approach of calculating them without implying differences in how they can be analysed (Smith & Kutas, 2015a).

The regression-based approach eliminates the need to split data for different events since rERPs for these events can be estimated simultaneously by fitting a single model based on the general equation for least squares linear regression:

$$y_i = \beta_1 \cdot x_{1i} + \beta_2 \cdot x_{2i} + \ ... + noise_i \quad (4)$$

The predictors x_1 and x_2 can be entered into the equation via different coding schemes that I will explain in the following.

1.3.1.1 Intercept

Explicitly including target trials as a predictor

$$x_{ti} = 1 \quad (5)$$

into equation (2) equals the results of averaging:

$$y_i = \beta_t \cdot x_{ti} + noise_i = \beta_t + noise_i \quad (6)$$

In this case, the predictor x_{ti} is called the intercept term since it has a value of 1 at every trial entered into the regression equation (Smith & Kutas, 2015a).

1.3.1.2 Dummy coding

This coding scheme benefits from the so-called "zero trick". Going along with the example of the oddball experiment, similar to averaging, we could deliberately bin the data and fit separate models for targets *t* and distractors *d* by including them in equation (6) as their respective intercept terms. Alternatively, we can add both predictors to the general least squares linear regression equation (4) and obtain multiple rERPs by simultaneously fitting two separate instances of the intercept-only model (6) to two independent data subsets. Therefore, we define the predictors as $x_t=1$ and $x_d=0$ for target trials and $x_t=0$ and $x_d=1$ for distractor trials. Then the least squares solution for β_t will represent the average of target trials (7), and β_d the average of distractor trials (8) (Smith & Kutas, 2015a):

$$y_i = \beta_t \cdot 1 + \beta_d \cdot 0 + noise_i = \beta_t + noise_i \quad (7)$$

$$y_i = \beta_t \cdot 0 + \beta_d \cdot 1 + noise_i = \beta_d + noise_i \quad (8)$$

1.3.1.3 Treatment coding

A slight but beneficial variation of dummy coding is treatment coding since it enables the definition of models in a non-redundant way. With this approach, all levels of an experimental factor except one, the reference level, are dummy coded. The reference level is added as an intercept term.

If targets are added as intercept, they are estimated equal to equation (7), and β_t values continue to represent the average of target trials. The dummy-coded distractors, however, are calculated as

$$y_i = \beta_t \cdot 1 + \beta_d \cdot 1 + noise_i = \beta_t + \beta_d + noise_i \quad (9)$$

Here β_d represents the difference between distractors to targets. All rERPs obtained so far, if plotted, are known as parent waveforms. Plotting β_d values, however, results in a difference wave. Consequently, a parent wave for distractors could be obtained from this model by adding β_d to β_t coefficients.

1.3.1.4 Modelling linear effects with slope rERPs

The regression approach can, unlike ERP averaging, also be applied to analysing continuous covariates like RT. Assuming we want to model the effect of RTs between 300 and 600 ms on target ERP estimates, we can normalise this range and add it to the regression equation as covariate x_{rt}. As a result, β_t can be interpreted as a baseline ERP estimate for an RT of 300 ms, while the amount that the ERP estimates for target stimuli are altered with each unit change in RT is represented by β_{rt}. The predicted target ERP for an RT of 330 ms would, according to this, be

$$y_i = \beta_t \cdot 1 + \beta_{rt} \cdot 0.1 + noise_i \quad (10)$$

or, similarly, for an RT of 450 ms

$$y_i = \beta_t \cdot 1 + \beta_{rt} \cdot 0.5 + noise_i \quad (11)$$

Slope ERPs, therefore, enable the modelling of categorical and continuous covariates simultaneously. Applying the zero trick here is advantageous if only a main effect of a covariate should be modelled. The RT covariate is then constrained to the same waveform for targets and distractors instead of having an interaction with trial types. Since RT is a proxy for the underlying neural processes, this makes sense if we do not expect differences in processing for targets and distractors. Dummy coding can furthermore be useful to constrain a continuous covariate like RT to only one categorical predictor, e.g. in go/no-go paradigms where the RT would get set to zero for no-go trials (Smith & Kutas, 2015a).

1.3.1.5 Modelling nonlinear effects with spline regression

The assumption of linear covariate effects confines slope ERPs. While it can be a reasonable approximation, this assumption is too restrictive in other cases. Recently, the linear model was combined with spline regression, based upon the generalised additive model (GAM) (Wood, 2017), to model nonlinear effects (Hendrix et al., 2017; Kryuchkova et al., 2012; Tremblay & Newman, 2015).

Here, the predictor x_{rt} is replaced by a set of *k* basis functions $f(x_{rt})$. Calculating their weighted sum

$$\sum_{k} \beta_k f_k(x_{rt}) \tag{12}$$

facilitates fitting nonlinear curves and therefore estimating nonlinear covariate effects. As before, the least squares regression finds the curve that represents the data best (Smith & Kutas, 2015b). Commonly used basis sets include the step-function (zero-degree B-spline) basis, polynomial basis, Fourier basis, and cubic (third-degree) B-spline basis (Figure 4). These lead to different curve fits.

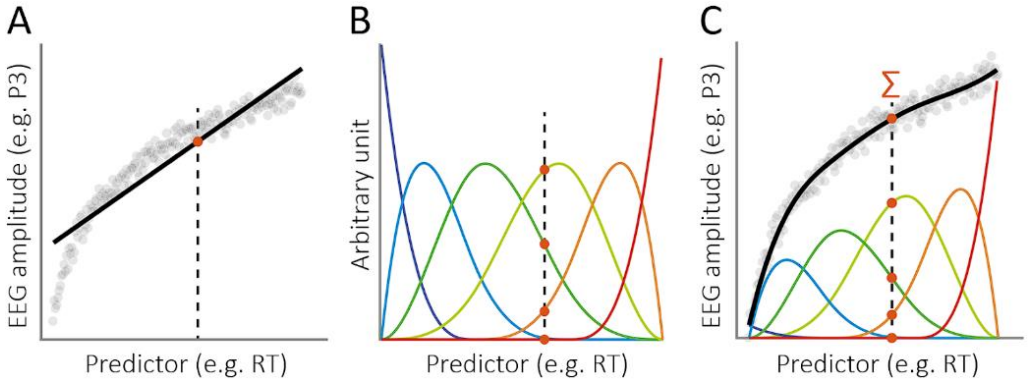

Figure 4. Modelling a nonlinear relationship with spline functions. A) A zero-degree B-spline basis set produces a linear fit that does not approximate the nonlinear relationship of a predictor (e.g. RT) and a dependent variable (e.g. EEG amplitude) well. B) A third-degree B-spline basis set with six overlapping spline functions distributed across the range of the predictor. Since each spline function is restricted to a certain range of the predictor, only three of the six predictor values (red dots) are non-zero. C) The sum of each spline weighted with its respective estimated beta value produces a smooth nonlinear fit that approximates the observed relationship between the predictor and the dependent variable well. Adapted from "Unfold: an integrated toolbox for overlap correction, nonlinear modelling, and regression-based EEG analysis" by B. V. Ehinger and O. Dimigen, 2019, PeerJ, 7, e7838. CC-BY 4.0.

Higher-order splines are a good choice since they produce smooth curves, similar to EEG signals, and allow to describe the underlying data sparsely. They are furthermore locally bounded, i.e. restricted to a certain range of the continuous predictor. Therefore, the fitted curve in a given range depends only on data near that range. An important consideration to achieve sensible β coefficients is the number *k* of basis functions that should be used to avoid under- or overfitting the data (Ehinger & Dimigen, 2019; Smith & Kutas, 2015b).

1.3.2 Mass univariate model

The mass univariate model has gained popularity for analysing datasets that combine multiple categorical and continuous covariates (Amsel, 2011; Hauk et al., 2006; Rousselet et al., 2008, 2009). This regression-based approach brings together the concepts just described. EEG data are first epoched around time-locking events to implement the mass univariate model, similar to the averaging approach. Afterwards, separately for all channels, a regression model is fit to each time point in the epoch. An exemplary mass univariate model for two events with treatment-coded predictors is depicted in Figure 5.

Going from regression terminology to the depicted matrix notation is straightforward. The general linear regression equation (4) written in matrix notation is:

$$y = X \cdot b + e \tag{13}$$

The dependent variable y represents measured EEG data points for equal time points τ relative to the onset of a time-locking event over epochs. The design matrix X contains one column per modelled event with a dummy- or treatment-coded predictor for each trial. The beta coefficients b are estimated by running the model for each time point τ, resulting in an rERP (Figure 5B) for each event. And the error term e is a vector of residuals that is minimised during the least squares fitting process to find the betas that together explain the EEG data best (Dimigen & Ehinger, 2021).

In its simpler forms, the mass univariate model enables obtaining multiple ERPs for categorical predictors by defining a single formula. Combinations of averaging and difference waves could achieve comparable results (Smith & Kutas, 2015a). The models' advantage over the averaging approach is that covariates like RT can be accounted for by including them as additional predictors to estimate their linear or nonlinear effects, as

described above. The limitation of this model is that there is no possibility of accounting for overlapping neural responses from adjacent events (Dimigen & Ehinger, 2021).

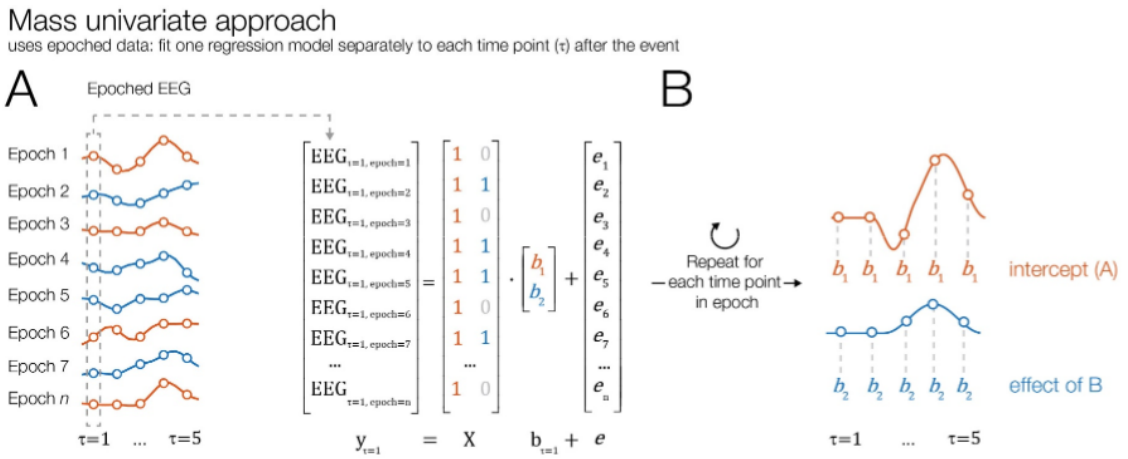

Figure 5. Illustration of the mass univariate model for EEG at a single electrode. (A) For each time point τ relative to the event onset of the epoched data y, a separate regression model is fit. The design matrix X contains one column for each event, with one predictor per trial (1 or 0) according to the chosen coding scheme. For the depicted treatment coding scheme, the first predictor is coded as an intercept term and represents the neural activity evoked by type A events. In contrast, the second predictor captures the effect of type B events. (B) Regression ERP (rERP) waveforms plotted from the beta coefficient vectors obtained by repeatedly running the model for each time point τ. From "Analyzing combined eye-tracking/EEG experiments with (non)linear deconvolution models." by O. Dimigen and B. V. Ehinger, 2020, bioRxiv. CC-BY-NC-ND 4.0.

1.3.3 Deconvolution model

The abovementioned methods cannot be used for overlap correction. A simple but insufficient method is to jitter ISIs to reduce overlap effects between adjacent events (Smith & Kutas, 2015b), having a similar effect as the random variation in RTs described above. Early deconvolution techniques based on Fourier transformation (Hansen, 1983) and the ADJAR algorithm (Woldorff, 1993) are restricted to a small number of events or cannot be applied to continuous predictors. The RIDE algorithm (Ouyang et al., 2011, 2015), which, unlike other methods, does not require designated event markers, but shows both of these limitations.

Another deconvolution method has been adapted from the analysis of the hemodynamic response in functional magnetic resonance imaging (fMRI) (Dale & Buckner, 1997). The advantage of this linear deconvolution approach based on least squares regression is that it is possible to model various event types and continuous covariates in a single model (Dimigen & Ehinger, 2021).

Smith and Kutas (2015b) showed with simulated data that not accounting for overlap produces wrong ERP estimates, while regression-based overlap correction enables recovering the correct waveform. Linear deconvolution has successfully been applied to account for overlapping potentials in the analysis of EEG and MEG time series (Dandekar et al., 2012; Dimigen & Ehinger, 2021; Lütkenhöner, 2010; Sassenhagen, 2019; Smith & Kutas, 2015b) and time-frequency (Litvak et al., 2013) studies.

That it allows overlap correction is another significant advantage of encoding more than one predictor in a regression equation, as opposed to averaging. To disentangle neural activity evoked by different event types in close temporal proximity, the waveforms for both must be estimated within a single model. This expands by-epoch regression to a model that eliminates epoching and is directly applied to continuous EEG data (Smith & Kutas, 2015b).

Predicated on the linear summation and LTI assumptions, the measured EEG represents the linear convolution of isolated neural responses that overlap if latencies of adjacent events are shorter than ERP durations. Deconvolution draws on the knowledge about event latencies to estimate the unknown isolated neural responses from the measured EEG (Ehinger & Dimigen, 2019).

This model can not only deal with the inter-trial variation of event latencies, it benefits from it. If stimulus sequences are invariable and persistently occur with equal ISIs, they are perfectly collinear, and no method can disentangle the neural responses (Smith & Kutas, 2015b). Mechanisms to break this perfect collinearity include the variation of stimulus sequences and the introduction of stimulus-onset asynchronies. Natural variation in RTs adds further latency variability (Ehinger & Dimigen, 2019; Smith & Kutas, 2015b). Smith and Kutas (2015b) demonstrated via a simulation that the true waveform of overlapping ERPs can be recovered in the presence of stimulus variation or latency jitter, while rERPs are most accurate if both are present.

Overlap correction makes again use of the zero trick. However, instead of dummy coding predictors, we are essentially dummy coding the regression equations from above, bringing many regression models together and building one giant model for each channel. Let us assume we want to model three events of the oddball task, a target stimulus *t* occurring at data point y_{21}, the button press b executed at data point y_{22}, and another target

stimulus that occurred at y_{25}. For simplicity, we model 5 latencies $l_{1\text{-}5}$ after the onset of each time-locked event. Then our linear regression model for overlap correction would be:

$$
\begin{aligned}
&\dots\\
&y_{20} = (\beta_t \cdot 0 + \beta_b \cdot 0)_{l1} + (\beta_t \cdot 0 + \beta_b \cdot 0)_{l2} + (\beta_t \cdot 0 + \beta_b \cdot 0)_{l3} + (\beta_t \cdot 0 + \beta_b \cdot 0)_{l4} + (\beta_t \cdot 0 + \beta_b \cdot 0)_{l5} + noise_i\\
&y_{21} = (\boldsymbol{\beta_t} \cdot \mathbf{1} + \beta_b \cdot 0)_{l1} + (\beta_t \cdot 0 + \beta_b \cdot 0)_{l2} + (\beta_t \cdot 0 + \beta_b \cdot 0)_{l3} + (\beta_t \cdot 0 + \beta_b \cdot 0)_{l4} + (\beta_t \cdot 0 + \beta_b \cdot 0)_{l5} + noise_i\\
&y_{22} = (\beta_t \cdot 0 + \boldsymbol{\beta_b} \cdot \mathbf{1})_{l1} + (\boldsymbol{\beta_t} \cdot \mathbf{1} + \beta_b \cdot 0)_{l2} + (\beta_t \cdot 0 + \beta_b \cdot 0)_{l3} + (\beta_t \cdot 0 + \beta_b \cdot 0)_{l4} + (\beta_t \cdot 0 + \beta_b \cdot 0)_{l5} + noise_i\\
&y_{23} = (\beta_t \cdot 0 + \beta_b \cdot 0)_{l1} + (\beta_t \cdot 0 + \boldsymbol{\beta_b} \cdot \mathbf{1})_{l2} + (\boldsymbol{\beta_t} \cdot \mathbf{1} + \beta_b \cdot 0)_{l3} + (\beta_t \cdot 0 + \beta_b \cdot 0)_{l4} + (\beta_t \cdot 0 + \beta_b \cdot 0)_{l5} + noise_i\\
&y_{24} = (\beta_t \cdot 0 + \beta_b \cdot 0)_{l1} + (\beta_t \cdot 0 + \beta_b \cdot 0)_{l2} + (\beta_t \cdot 0 + \boldsymbol{\beta_b} \cdot \mathbf{1})_{l3} + (\boldsymbol{\beta_t} \cdot \mathbf{1} + \beta_b \cdot 0)_{l4} + (\beta_t \cdot 0 + \beta_b \cdot 0)_{l5} + noise_i\\
&y_{25} = (\boldsymbol{\beta_t} \cdot \mathbf{1} + \beta_b \cdot 0)_{l1} + (\beta_t \cdot 0 + \beta_b \cdot 0)_{l2} + (\beta_t \cdot 0 + \beta_b \cdot 0)_{l3} + (\beta_t \cdot 0 + \boldsymbol{\beta_b} \cdot \mathbf{1})_{l4} + (\boldsymbol{\beta_t} \cdot \mathbf{1} + \beta_b \cdot 0)_{l5} + noise_i\\
&y_{26} = (\beta_t \cdot 0 + \beta_b \cdot 0)_{l1} + (\boldsymbol{\beta_t} \cdot \mathbf{1} + \beta_b \cdot 0)_{l2} + (\beta_t \cdot 0 + \beta_b \cdot 0)_{l3} + (\beta_t \cdot 0 + \beta_b \cdot 0)_{l4} + (\beta_t \cdot 0 + \boldsymbol{\beta_b} \cdot \mathbf{1})_{l5} + noise_i\\
&y_{27} = (\beta_t \cdot 0 + \beta_b \cdot 0)_{l1} + (\beta_t \cdot 0 + \beta_b \cdot 0)_{l2} + (\boldsymbol{\beta_t} \cdot \mathbf{1} + \beta_b \cdot 0)_{l3} + (\beta_t \cdot 0 + \beta_b \cdot 0)_{l4} + (\beta_t \cdot 0 + \beta_b \cdot 0)_{l5} + noise_i\\
&\dots
\end{aligned}
\tag{14}
$$

With this model, data point y_{25} would therefore be encoded as the linear sum of stimulus-evoked neural activity occurring at exactly this data point, stimulus-evoked activity from five samples prior, and response-evoked activity from four samples prior (Smith & Kutas, 2015b). This example is depicted in Figure 6 illustrating the deconvolution model more comprehensively. The model is expressed in matrix notation as:

$$y = X_{dc} \cdot b + e \tag{15}$$

For overlap correction, the dependent variable *y* is the continuous EEG data. Whereas for the mass univariate model the design matrix X contained one predictor per trial and event, the time-expanded design matrix for deconvolution X_{dc} consists of one predictor per data point *y*, event, and time point τ relative to event onset.

Instead of modelling five time points, as in the example above and Figure 6, for an actual experiment, all samples within a time window of 1-2 s would be included. Assuming the sampling rate is 250 Hz and the chosen time window is -500 to 1000 ms, then X_{dc} would contain 375 predictors per event in each row. Sticking to the example of modelling targets and responses, 375 predictors for each event would be concatenated horizontally, resulting in 750 columns.

Similar to before, when the model is solved, the error term e is minimised during the least squares fitting process to obtain the unknown beta coefficients b that together explain the EEG data best (Ehinger & Dimigen, 2019). A unique solution is found due to variable stimulus sequences, latency jitter, or both (Ehinger & Dimigen, 2019; Smith & Kutas, 2015b).

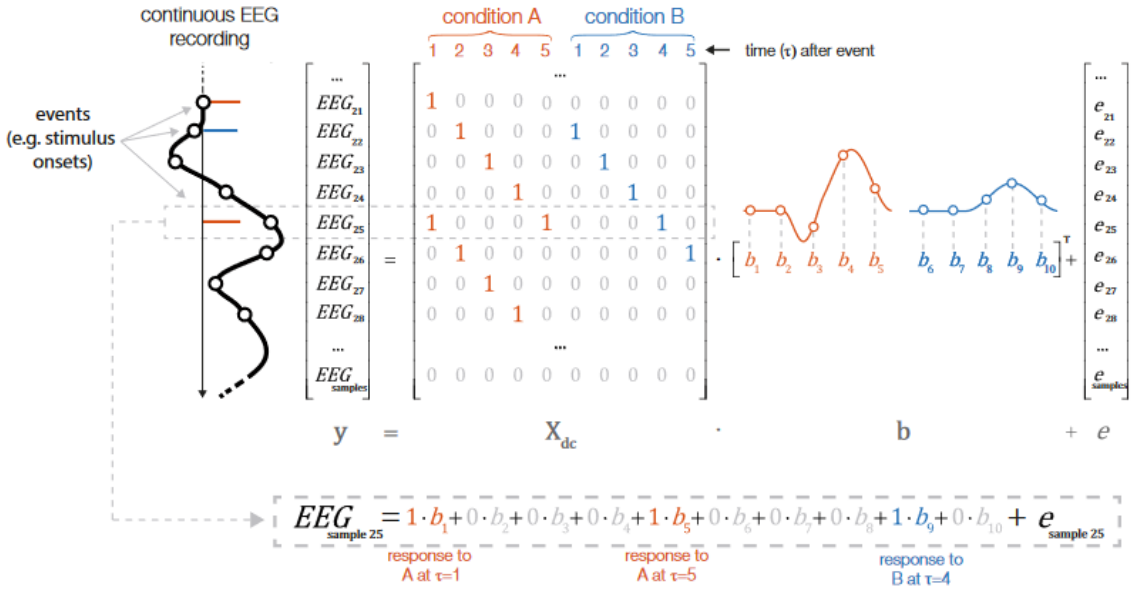

Figure 6. Linear deconvolution for overlap correction. To estimate the beta coefficients b, regression ERPs (rERPs) that represent the unknown evoked neural responses, the continuous EEG data y is entered into the model, and the time-expanded design matrix Xdc is created. Xdc consists of predictors for all local time points τ that are added around each event, here only five time points. In this example, EEG sample 25 represents the sum of neural responses to two events of type A at time points 1 and 5 after the events and to an event of type B at time point 4 after the event. If latency jitter, variable stimulus sequences, or both are present, the least squares model fit will represent the betas that represent y best while minimizing the error e. From "Unfold: an integrated toolbox for overlap correction, nonlinear modelling, and regression-based EEG analysis" by B. V. Ehinger and O. Dimigen, 2019, PeerJ, 7, e7838. CC-BY 4.0.

Recently, the combination of linear deconvolution with spline regression (GAM) has been shown to allow for overlap correction and modelling of nonlinear covariate effects. Therefore, the additional predictor is added to the designmatrix. This further improving the accuracy of estimated ERPs (Dimigen & Ehinger, 2021; Ehinger & Dimigen, 2019).

1.4 THE P300 COMPONENT

The P300, also known as 'P3' or 'P3b', is commonly described as a large-amplitude ERP component originating from centroparietal brain regions, including primary sensory-motor areas, and can be observed independent of sensory modality (Di Russo et al., 2016; Twomey et al., 2015). It appears as a late-positive wave that peaks between 300 to 600 ms after the presentation of a rare task-relevant stimulus, meaning subjects have to respond in a covert (e.g. counting) or overt (e.g. button press) manner to target stimuli (Twomey et al., 2015).

The P300 is typically evaluated by measuring its amplitude and latency. Its amplitude has been shown to depend on the perceived prior probability of the category in which a subject is instructed to classify the stimulus. Therefore, a subject's expectation about an upcoming event affects P300 amplitude and latency based on preceding probabilities. Stimuli appearing with a higher chance are identified faster, and the amplitude of the P300 is larger the rarer the stimulus (Duncan-Johnson & Donchin, 1977). P300 amplitude has further been shown to decrease with the presentation of subsequent targets (Lammers & Badia, 1989) and to be larger for detected than undetected or falsely reported targets (Hillyard et al., 1971).

The P300 signal has received the most research attention throughout EEG studies over the past five decades (Kelly & O'Connell, 2015), generating much interest because of its seeming universality. Following the initial discovery in 1965 (Sutton et al., 1965), it got associated with a range of cognitive processes, including the subjects' degree of confidence in a decision (Hillyard et al., 1971; Squires et al., 1973), context updating (Donchin & Coles, 1988), event-categorization (Kok, 2001), neural inhibition (Polich, 2007), and decision making (Twomey et al., 2015). The P300 has further been shown to be sensitive to various brain disorders such as depression (Santosh et al., 1994), Alzheimer's disease and other dementias (Rossini et al., 2007), as well as obsessive-compulsive disorder (Raggi et al., 2021). More recently, the P300 signal gained increasing interest in brain-computer interface (BCI) applications like P300 spellers developed by Farwell and Donchin (1988) and position control of robotic arms (Bhattacharyya et al., 2014; Rakshit et al., 2020).

There is growing evidence that the P300 component intermediates between stimulus processing and response preparation as a decision variable. However, despite extensive research, the P300's usefulness as an interpretable neurocognitive marker has been severely constrained because no single model has obtained unequivocal empirical validation (Twomey et al., 2015). This inability to reach a consensus regarding the precise role of the P300 has primarily been attributed to RT variability and signal overlap (Kelly & O'Connell, 2013, 2015; Twomey et al., 2015).

1.5 GOALS OF THIS STUDY

This study investigates the effects of temporal overlap and varying event durations on neural responsesFor the analysis in this study, RTs were modelled for stimuli and responses simultaneously.

This study aims to analyse the effects of overlap and varying event durations on ERP waveforms by comparing estimates of different data-analytic methods. To this end, I recorded EEG data from participants conducting a classic oddball task. For data analysis, the Unfold.jl toolbox by Ehinger and Dimigen (2019) facilitates regression-based EEG analyses and provides the options to implement the models introduced above. I first implemented the mass-univariate model that produced ERP estimates that could have also been obtained by averaging as a sanity check to compare the results to a study that implemented the traditional ERP averaging approach. The deconvolution model was then applied to the data to investigate the effects of overlapping potentials. Finally, expanding this model by spline regression to a GAM enabled the additional modelling of RT effects on stimulus and response rERPs.

With this approach, I hypothesised that the amplitude difference of the P300 component between conditions in stimulus- and response-locked ERP estimates, elicited during a classical oddball experiment, stems from an interaction of overlap and varying RTs.

2 MATERIALS & METHODS

The local ethics committee of the University of Stuttgart approved this study.

2.1 PARTICIPANTS

Over the course of this study, EEG data were recorded from 38 right-handed participants aged 21 to 36 years (mean 27.2, SD 3.5; 14 female). Each participant had normal (n=26) or corrected-to-normal vision and passed an eyesight test confirming 6/6 vision prior to the experiment.

All participants completed another task in the same session. The order in which these were carried out was randomised. The participants gave written informed consent and received 15€/hour of monetary compensation. They were verbally queried for exclusion criteria, which included tinnitus, photosensitive migraine or epilepsy, and other severe neurological or psychiatric disorders.

2.2 APPARATUS

Participants were seated in a dimly lit room on a comfortable, rotation- and translation-locked chair. The LED display (ACER Nitro XV252QF) for stimulus presentation was placed at a viewing distance of approximately 90 cm and was controlled via a Tower-PC (HP EliteDesk 800 G6, GPU: AMD Radeon RX 550X). Stimuli were presented with Psychtoolbox-3 (Brainard, 1997; Kleiner et al., 2007) via Matlab 2022a (The MathWorks Inc.). Participants responded with their left and right index finger using a response box (MilliKey SR-5 r1) placed on the table in front of them. The two buttons relevant to respond to experimental stimuli were marked in blue and yellow.

2.3 EXPERIMENTAL TASK

An active visual oddball task was carried out to elicit the P300 component. This paradigm is commonly implemented as an auditory or visual task. In this study, a visual oddball experiment was carried out because vision is frequently regarded as the most important human sense (Hutmacher, 2019) and is the dominant sense for movement control

(Glickstein, 2000). The experimental paradigm was adopted from the ERP Core (Kappenman et al., 2021a).

Stimuli for this experiment were the five upper-case letters A, B, C, D, and E, presented in Roboto Mono font, and subtending approximately 2.5 x 2.5° of visual angle. The screen was filled with a grey background. Letters were superimposed over a fixation cross in the screen centre, which participants were instructed to fixate on throughout the task.

The experiment consisted of ten blocks with 120 trials each. Instead of 200 trials (Kappenman et al., 2021a), in this study, 1200 trials were recorded with each subject to acquire enough data and avoid collinearity due to the implemented analysis approach (Smith & Kutas, 2015b). At the beginning of each block, one of the letters was assigned the target, while the other four were distractors. Target-response mappings, i.e. which button (blue or yellow) to press for the target and distractor letters, were randomised between blocks and assigned at the start of each block. In every trial, a letter was presented for 200 ms. While in the ERP Core ISIs lasted between 1200 to 1400 ms (Kappenman et al., 2021a), in this study, the stimuli were followed by an ISI that varied pseudorandomly between 700 to 2500 ms with a mean of 1100 ms (Figure 7). This adjustment was based on the fact that increased ISI variability improves the model fit when overlap correction is applied to EEG data (Smith & Kutas, 2015b). Each letter had a probability of 20% to occur on a given trial and was designated the target for two blocks while belonging to the distractor class in the other eight blocks. The sequence of letter presentation was randomised except that the presentation of subsequent targets was prevented such that at least one distractor was shown between targets. Habituation would otherwise lead to a P300 amplitude decrease and latency increase (Lammers & Badia, 1989).

Participants were instructed to respond as quickly and accurately as possible. They controlled the length of pauses between blocks by themselves. All participants completed a short example run of two blocks with 20 trials to get familiarised with the task.

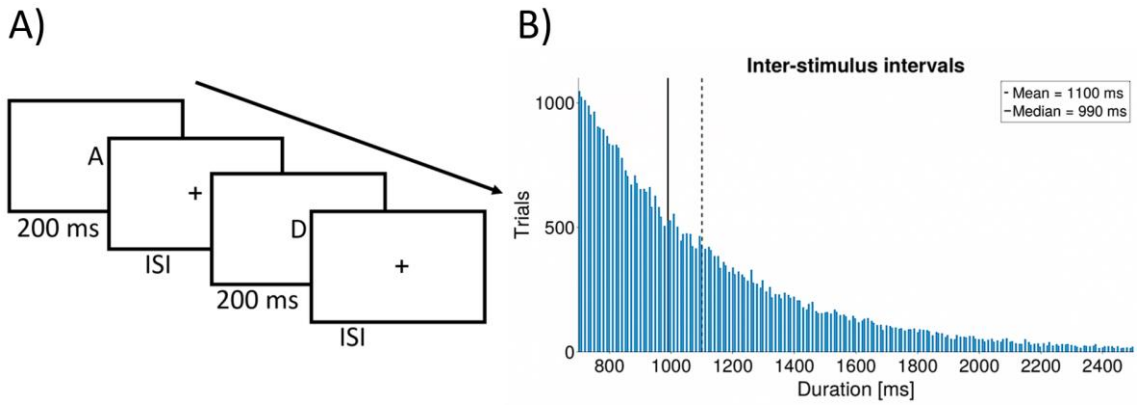

Figure 7. A) Schematic of oddball task. Stimuli (letters) were presented for 200 ms. Letters were separated by inter-stimulus intervals (ISIs) of varying duration where only a small fixation cross was visible. B) Distribution of ISIs in the range of 700 to 2500 ms (mean = 1100 ms, median = 990 ms).

2.4 EEG RECORDING & DATA PREPROCESSING

An AntNeuro (Enschede, Netherlands) System comprised of an eego™ sports amplifier (EE-225) and waveguard™ original cap (CA-203.s1) was used to record continuous EEG and electrooculogram (EOG) data. The 128-channel cap was placed according to the 10/5 system, and data were recorded from 60 Ag/AgCl scalp electrodes (FP1, FPz, FP2, AF7, AF3, AF4, AF8, F7, F5, F3, F1, Fz, F2, F4, F6, F8, FT7, FC5, FC3, FC1, FCz, FC2, FC4, FC6, FT8, M1, T7, C5, C3, C1, Cz, C2, C4, C6, T8, M2, TP7, CP5, CP3, CP1, CP2, CP4, CP6, TP8, P7, P5, P3, P1, Pz, P2, P4, P6, P8, PO7, PO3, POz, PO4, PO8, O1, O2). Additionally, two horizontal EOG ring electrodes were placed lateral to the outer canthi of the left (HEOGL) and right (HEOGR) eye, and two vertical EOG electrodes above (VEOGU) and below (VEOGL) the midline of the left eye. The GRD electrode was placed at the left earlobe, and CPz was used as an online reference. Data were digitised at a sampling rate of 1000 Hz.

Data were preprocessed in MATLAB 2021a (The MathWorks Inc.) with a custom script based on (Pernet et al., 2021). First, channel locations were added, and the raw data were downsampled to 256 Hz. Afterwards, 50 Hz line noise, unidentified 8 Hz noise and their harmonics were cleaned with Zapline-plus (de Cheveigné, 2020; Klug & Kloosterman, 2022). Channels with a flatline of 5 continuous seconds or more were removed. Data were re-referenced offline to the average of channels P7 and P8. Subsequently, adaptive mixture independent component analysis (AMICA) (Hsu et al.,

2018) was run, and the resulting weights were applied to the data to remove artefactual components. Muscle, eye, and heart artefacts, line, channel, and other noise that were flagged as artefacts with at least 80% confidence by the ICLabel algorithm (Pion-Tonachini et al., 2019) were removed. Artefact subspace reconstruction (ASR) (Mullen et al., 2015) then marked short-time high-variance signals in the continuous data. Experimental events affected by these artefacts were removed from the design matrix of the models later on. Two subjects were excluded from further analyses because of too many artefacts in the EEG data. Finally, bad channels were interpolated, and data were high-pass filtered at 0.1 Hz.

2.5 BEHAVIOURAL ANALYSIS

For behavioural and further analyses, trials where participants made no or more than one response were removed, as well as trials where the response was faster than 200 ms or slower than 1 s. Accuracy was then calculated as the proportion of correct trials divided by all remaining trials. Trials where participants made incorrect behavioural responses were subsequently excluded from further analyses. Participants had to exhibit an overall accuracy of at least 75% and an accuracy of at least 50% for both target and distractor conditions, similar to the ERP Core (Kappenman et al., 2021a). Two subjects were excluded from further analyses because they did not meet the accuracy threshold for the target condition (44.06% and 48.89%).

2.6 EEG ANALYSIS

Data analysis was carried out in Julia (Bezanson et al., 2017). The P300 component was analysed at Pz, as this is the commonly used channel throughout the literature and because the P300 amplitude is greatest at this location (Kappenman et al., 2021a; Luck, 2014).

The models were implemented according to the dummy coding scheme using the Unfold.jl toolbox (Ehinger & Dimigen, 2019). For the mass univariate model, the EEG data were epoched, and the design matrix X was created. Then the model was fit to each time point and channel. In the Unfold.jl toolbox, models are specified according to the commonly used Wilkinson notation (Wilkinson & Rogers, 1973). The model was defined as follows:

$$EEG \sim 0 + target + distractor + bp\_target + bp\_distractor \quad (16)$$

Here, bp is an abbreviation for a button press, indicating the response to target and distractor stimuli.

The deconvolution model for overlap correction was fit to the continuous EEG data separately for each channel without epoching. The time window comprised 2 s (513 samples) centred on event onset. The model was:

$$EEG_{stimulus} \sim 0 + target + distractor \quad \{for\ stimulus\ onset\ events\} \quad (17)$$

$$EEG_{response} \sim 0 + bp\_target + bp\_distractor \quad \{for\ manual\ button\ press\ events\} \quad (18)$$

The deconvolution model was extended to a GAM by including RT as an additional predictor, modelled with five third-degree B-spline basis functions to analyse RT effects:

$$EEG_{stimulus} \sim 0 + target + distractor + spl(RT,5) \quad \{for\ stimulus\ onset\ events\} \quad (19)$$

$$EEG_{response} \sim 0 + bp\_target + bp\_distractor + spl(RT,5) \quad \{for\ manual\ button\ press\ events\} \quad (20)$$

With this model, RT was restricted to the same effect on rERPs for target and distractor, separately for stimuli and responses.

Regression-ERPs were baseline corrected relative to the 200 ms interval prior to event onset. Target-minus-distractor difference waves were obtained by subtracting the rERPs for distractors from those for targets.

2.7 STATISTICAL ANALYSIS

P300 peak latencies were evaluated in a 300 to 600 ms time window post-stimulus, and in a 100 ms time window centred on response execution. Therefore the robust peak finder function provided by MNE-Python (Gramfort et al., 2013) was applied to within-subject target-minus-distractor difference waves. If more than one significant peak was returned, the peak with maximal amplitude was chosen. P300 mean amplitude was then calculated as the winsorised mean of model estimates in a 300 ms time window centred on each subject's P300 peak latency. Subsequently, bootstrap resampling was applied to establish the 95% confidence intervals for P300 mean amplitudes of the stimulus and response difference waves.

3 RESULTS

3.1 BEHAVIOUR

The 34 participants had a mean RT of 409.71 ± 54.31 ms in response to target stimuli. Responses to distractors were faster, with a mean RT of 340.37 ± 62.62 ms. The mean accuracy for targets was 83.72 ± 12.13 %. Distractors were rarely missed, with a mean accuracy of 99.25 ± 0.76 %.

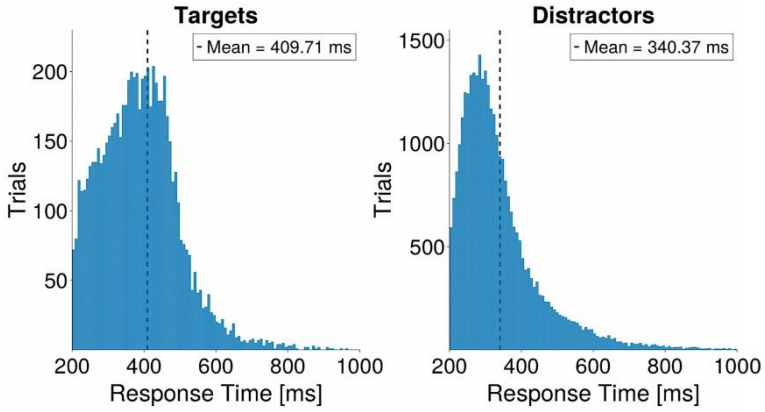

Figure 8. Distribution of response times (RTs) during the visual oddball task. A) Mean RT for target stimuli was 409.71 ms across subjects. B) RTs for distractor stimuli were faster, with a mean of 340.37 ms.

3.2 EFFECTS OF OVERLAP AND VARYING RESPONSE TIMES

The stimulus-locked P300 peaked at a latency of 448.53 ms when estimated from the mass univariate model, at 421.19 ms for the deconvolution model, and at 430.15 ms for the GAM. The response-locked P300 peak was observed at a latency of 10.57 ms in the difference wave of the mass univariate model and the GAM. For the deconvolution model, the peak was at 11.26 ms (Table 1).

The P300 mean amplitude of the stimulus-locked difference wave was 2.484 µV, 95% CI [1.976, 3.005] for the mass univariate model. For the deconvolution model, the mean amplitude decreased to 1.513 µV [1.169, 1.881]. Including RTs as a predictor led to a slight increase in mean amplitude to 1.742 µV [1.376,2.064] for the GAM. Scalp topographies showed brain activity primarily located over parietal regions (Figure 9).

Table 1. Peak latency and mean amplitude of the P300 component. P300 peak latency is the mean latency of all subjects' maximal significant P300 peaks (standard deviations in parentheses). P300 mean amplitudes were obtained by bootstrapping within-subject target-minus-distractor difference waves, and 95% confidence intervals (CI) were calculated. Statistics were calculated separately for each event type (stimulus and response) for the mass univariate model, deconvolution model, and generalised additive model (GAM).

Model	Event type	P300 peak latency [ms]	P300 mean amplitude [µV] & 95% CI
Mass univariate model	Stimulus	448.53 (68.97)	2.484 [1.976, 3.005]
	Response	10.57 (26.13)	1.423 [1.074, 1.934]
Deconvolution model	Stimulus	421.19 (70.79)	1.513 [1.169, 1.881]
	Response	11.26 (25.32)	0.794 [0.347, 1.188]
Generalised additive model	Stimulus	430.15 (79.41)	1.742 [1.376, 2.064]
	Response	10.57 (20.97)	0.436 [0.123, 0.743]

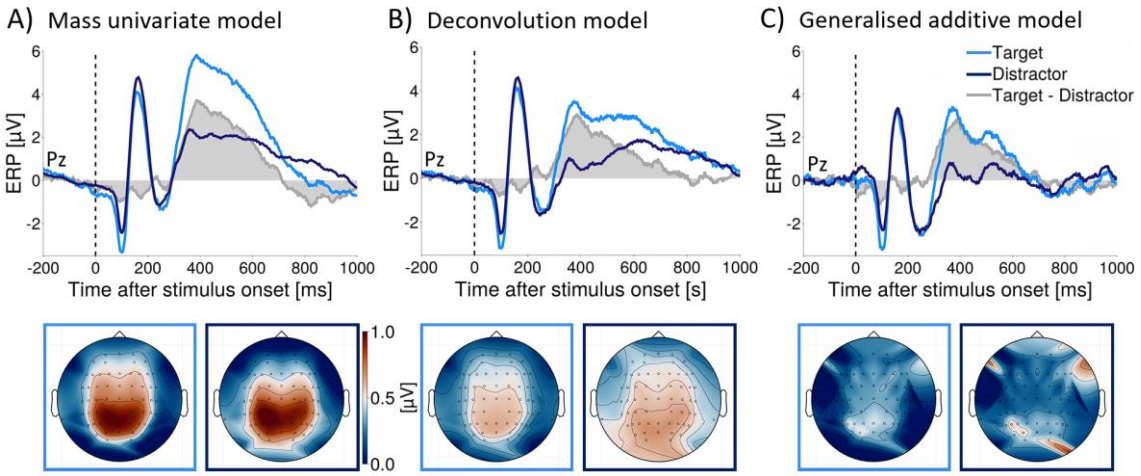

Figure 9. Stimulus-locked grand average regression-ERPs (rERPs) and scalp topographies. In the upper panel, rERPs for targets (light blue) and distractors (dark blue), as well as target-minus-distractor difference waves (grey), are illustrated at channel Pz. In the lower panel, scalp topographies for targets (light blue, left) and distractors (dark blue, right) are displayed for the time frame during which P300 mean amplitude was calculated. The dotted vertical line at 0 ms marks the stimulus onset. A) rERPs obtained from the mass univariate model. B) rERPs estimated with the deconvolution model for overlap correction. C) rERPs from the generalised additive model (GAM) were obtained by adding response time (RT) as a predictor to the deconvolution model. Scalp topographies show brain activity primarily located over parietal regions.

The response-locked P300 mean amplitude of the difference wave obtained from the mass univariate model was 1.423 µV [1.074, 1.934]. For the deconvolution model, the amplitude was smaller at 0.794 µV [0.347, 1.188]. The mean amplitude decreased further to 0.436 µV [0.123,0.743] in the GAM. Brain activity was again confined to parietal regions (Figure 10).

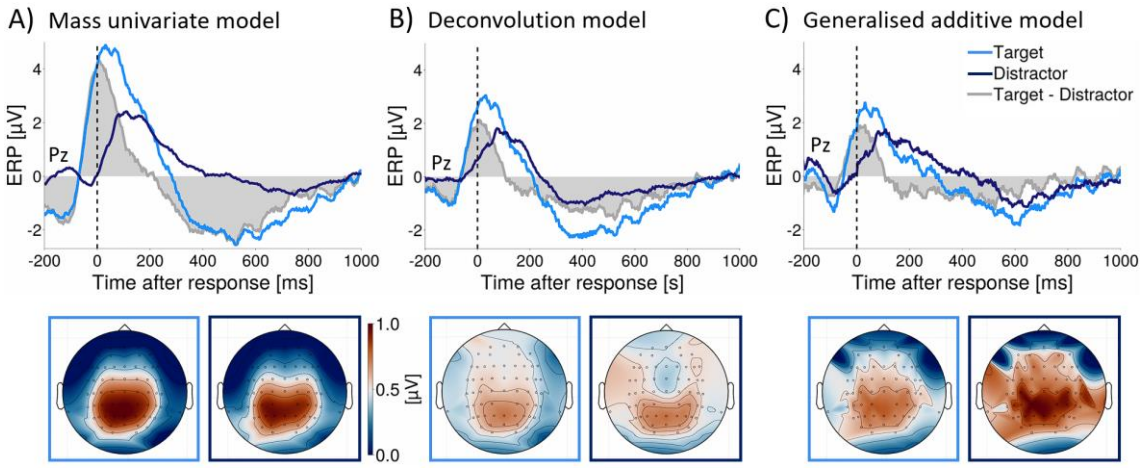

Figure 10. Response-locked grand average regression-ERPs (rERPs) and scalp topographies. The upper panel displays rERPs for targets (light blue) and distractors (dark blue), as well as target-minus-distractor difference waves (grey). The lower panel illustrates scalp topographies for the P300 component belonging to targets (light blue, left) and distractors (dark blue, right). The dotted vertical line at 0 ms marks response execution. A) rERPs obtained from the mass univariate model. B) rERPs estimated with the deconvolution model for overlap correction. C) rERPs from the generalised additive model (GAM). Scalp topographies for the P300 indicate brain activity located mainly at parietal regions.

A more detailed analysis with the GAM revealed how the P300 amplitude of overlap corrected rERPs varied with RT. Effects were evaluated for RTs between 360 to 420 ms (Figure 11). Stimulus-locked rERPs at the P300 peak latency of 430 ms decreased by 0.517 µV with this 60 ms change in RT. The potential of rERPs was largest for fast RTs and decreased with increasing RTs. RT had a mostly linear effect on P300 amplitudes from 360 to 390 ms. From 390 to 420 ms, the P300 amplitude decreased nonlinearly with increasing RT. Therefore, a unit change in RT led to a greater decrease in P300 amplitude for slow compared to fast RTs.

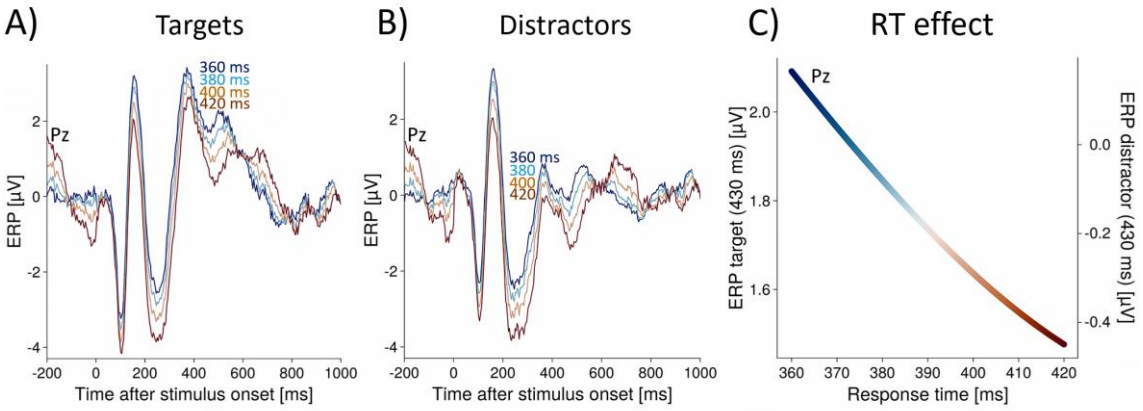

Figure 11. Effects of response time (RT) on stimulus-locked regression ERPs (rERPs) estimated with the generalised additive model (GAM). Displayed are the effects of RTs between 360 to 420 ms. P300 amplitudes for A) targets and B) distractors were greatest for fast RTs and lowest for slow RTs. C) P300 amplitudes at the peak latency of 430 ms decreased primarily linearly for RTs between 360 and 390 ms and nonlinearly at slower RTs.

The change in P300 amplitude was greater in response-locked than stimulus-locked rERPs. With a 60 ms change in RT from 360 to 420 ms, the amplitude at 12 ms increased by 1.278 µV. RT had the opposite effect on response-locked compared to stimulus-locked rERPs. While stimulus-locked amplitudes were greatest for fast RTs, they were the smallest in response-locked rERPs when subjects responded quickly. The P300 amplitude at 12 ms increased nonlinearly with increasing RTs (Figure 12).

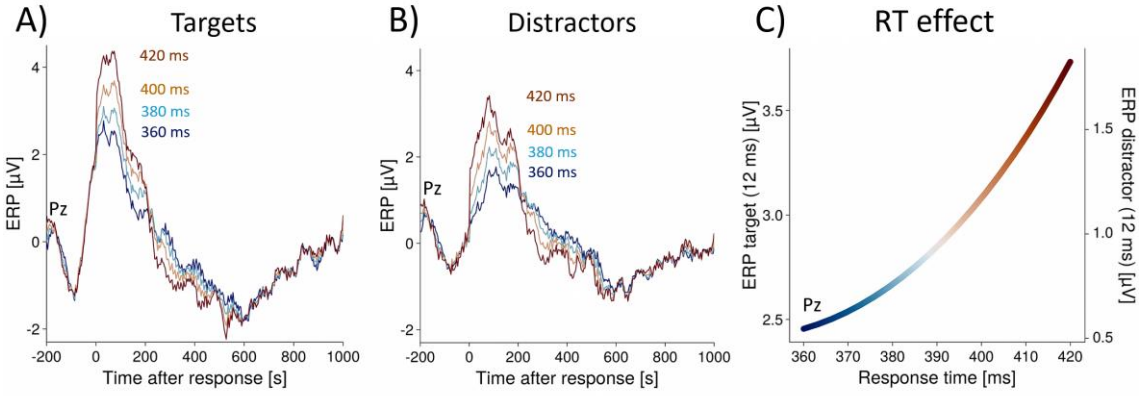

Figure 12. Effect of response time (RT) on response-locked regression-ERPs (rERPs). The effects of RTs between 360 to 420 ms on amplitude are displayed for A) target and B) distractor rERPs. The P300 component of targets and distractors had the smallest amplitude

4 DISCUSSION

Three regression-based models were implemented to investigate the effects of overlap and event duration on neural responses. The mass univariate model produces mathematically equal results to the classical ERP averaging approach (Smith & Kutas, 2015a), thus facilitating comparisons with previous studies. The deconvolution model was implemented to disentangle neural responses evoked by stimuli and responses and enables to analyse effects of overlapping neural responses. The deconvolution model was expanded to a GAM by including RT as an additional predictor modelled via spline regression to investigate the effects of varying RTs on rERPs.

4.1 BEHAVIOUR

In this study, I replicated the visual oddball paradigm from the ERP Core (Kappenman et al., 2021a), with minor adjustments as pointed out in section 2.3. Comparing behavioural results (Kappenman et al., 2021b), measures for mean RT and accuracy for target and distractor conditions were similar and within the standard deviations of the respective other study. The most noticeable difference was that for targets, the mean RT was 37.71 ms faster, and the accuracy was 6.09% lower in this study. This can be explained by a speed-accuracy trade-off (Gold & Shadlen, 2007). Subjects were instructed to maximise speed and accuracy but may individually perceive one instruction as more valuable than the other, leading to this difference.

4.2 COMPARISON TO ERP CORE

The here implemented mass univariate model produces mathematically equal results to the traditional ERP averaging approach (Smith & Kutas, 2015a). It thus facilitates the comparison of ERP estimates between this study and the ERP Core, where EEG data were analysed using ERP averaging (Kappenman et al., 2021a).

Grand average scalp topographies of mean P300 amplitude of parent waveforms for targets and distractors reveal similar localisation of neural responses confined to parietal brain regions. P300 peak latency at 408.89 ± 70.48 ms in the ERP Core (Kappenman et al., 2021a), and 448.53 ± 68.97 ms in the recent study, were again within standard deviations of each other study.

An important difference between the studies was observed for ERP estimates of stimulus-locked target-minus-distractor difference waves. The mean amplitude of the stimulus-locked P300 was 6.29 µV in the ERP Core (Kappenman et al., 2021a). In this study, it was much smaller at only 2.48 µV. This may, in part, be due to the high inter-trial latency jitter observed in ERP images during data analysis. However, sanity checks regarding the reason for this difference did not lead to a conclusion and require further investigation.

4.3 DECONVOLUTION

A comparison of rERPs obtained from the mass univariate and deconvolution models reveals the effects of overlapping neural responses. The mean amplitude of the P300 decreased significantly with overlap correction in both stimulus- and response-locked rERPs. This is in coherence with the behavioural results. Since mean RTs were 340.37 ms and 419.71 ms for targets and distractors, respectively, neural responses related to stimulus onsets strongly overlapped with those of the subsequent response. Due to this high amount of overlap it makes sense that overlap had a significant effect on rERPs. The large effect of overlap on ERP estimates is evident when comparing the waveforms of Figure 9 A) to B) and Figure 10 A) to B).

Smith & Kutas (2015b) confirmed with a simulation that the overlap corrected rERPs closely resemble the true ERP waveform, while the mass univariate model and, thus, ERP averaging fail to retrieve the true shape of ERPs. Overlap correction is, therefore, crucial to disentangle stimulus- and response-locked neural responses to accurately estimate ERPs. This generalises to all EEG studies where neural responses overlap due to events occurring in close temporal proximity, both due to experimental design or the analysis of naturalistic situations. However, overlap correction with the linear model requires known event latencies and enough data to avoid collinearity (Smith & Kutas, 2015a).

4.4 RESPONSE TIME MODELLING

To the best of my knowledge, this is the first study to analyse RT effects by modelling overlap and RT in one GAM simultaneously for stimulus- and response-locked brain

activity. Twomey et al. (2015) analysed RT effects during an oddball task, however, without overlap correction of the data and by dichotomising RTs, i.e. dividing them into slow and fast RT bins, which produces a suboptimal fit of the RT effect (Dimigen & Ehinger, 2021). Smith & Kutas (2015b) overlap corrected their data of a go/no-go task. However, due to collinearity, they had to estimate the response-locked rERP based on the assumption that the stimulus-locked ERP did not vary with RT. This would attribute all the unexplained variance in the overlap-corrected rERPs to the stimulus-locked ERP.

Modelling RT with the GAM had opposite effects on stimulus- and response-locked rERPs. P300 mean amplitude increased stimulus-locked while it decreased response-locked. The response-locked ERP is understood to resemble the brain activity related to response preparation and execution (Ehinger & Dimigen, 2019). The observation that RT affects response-locked rERPs more may thus be attributed to the fact that RT is the direct result of the neural processes that constitute the response-locked ERP and determine the latency of response execution.

While overlap and RT have been shown to affect rERPs, the initial hypothesis was rejected. The P300 mean amplitude for the stimulus-locked difference wave was 1.742 µV, 95% CI [1.376, 2.064], indicating that target and distractor rERPs differed significantly. The response-locked P300 amplitude estimated with the GAM was 0.436 µV [0.123, 0.743]. Therefore, it cannot be concluded that the amplitude difference between conditions stems from an interaction of overlap and varying RTs. Furthermore, since these statistical results are not significantly different from those obtained for the deconvolution model, it can be concluded that overlap had a significant effect on P300 mean amplitude, while there is only a small effect of RT on rERPs. This is in line with studies that showed that while latency jitter has effects on ERP amplitude, it is rather small for the oddball task (Cohen & Polich, 1997; Karniski & Clifford Blair, 1989; Michalewski et al., 1986).

A more detailed investigation of varying event durations revealed that RT affects the P300 amplitude nonlinearly at its peak latency (Figures 11C and 12C). This has an important implication in that it directly contradicts one of the basic assumptions of EEG analyses. Traditional ERP averaging and deconvolution models assume invariance of ERPs across trials of a given condition independent of overlap. The observations made in

this study that RT affects rERP amplitudes nonlinearly suggest that this assumption is incorrect and that cortical information processing differs between trials, as has been assumed based on RT variability across trials (Dimigen & Ehinger, 2021). It furthermore underlines the importance of enabling nonlinear relationships between covariates and ERP estimates through the correct model choice. Constraining predictors to a linear effect may bias analysis results otherwise (Dimigen & Ehinger, 2021).

Consistent with Twomey et al. (2015), the stimulus-locked P300 amplitude decreased as a function of RT and was the smallest for slow RTs (Figure 11). This was explained by the observation that the P300 component is most tightly time-locked to the response, which leads to smaller stimulus-locked amplitudes (Twomey et al., 2015). The argument can be supported by comparing the rERPs of individual models in Figures 9 and 10. The P300 component is narrower in response-locked rERPs, as expected for components that are more precisely time-locked to the response (Luck, 2014). Another similarity with that study is the relation between the P300 build-up rate and RT. Investigation of the response-locked P300 rERPs discloses a faster build-up rate for fast RTs (Figure 12 A and B). This supports the argument that the P300 may be a decision variable. However, the nonlinear effect of RT on the response-locked P300 amplitude at peak latency directly contradicts another criterion for this functional role of the P300. A key characteristic of a decision variable is that it determines behaviour via a boundary-crossing criterion (Kelly & O'Connell, 2013, 2015; O'Connell et al., 2012; Twomey et al., 2015). Instead of reaching a stereotyped amplitude immediately before response execution, in the current study, the P300 peak was observed at a latency of 10.57 ms after the response, and its amplitude was dependent on RT.

4.5 LIMITATIONS

This study has several limitations. The signal-to-noise ratio of the recorded EEG data is suboptimal. During preprocessing, noise was noticed in the data, the origin of which has not been traced back yet. Cleaning for 8 Hz and its harmonics with Zapline-plus provided the best results. However, in some recordings, small peaks remained.

Additionally, for many subjects, an unusually high amount of muscle artefacts was detected by the AMICA algorithm. Furthermore, for some recordings, ASR detected

numerous artefacts that affected only one or a few samples. The reason why they were marked as artefacts is unclear.

4.6 CONCLUSION

The EEG dataset recorded in this study exhibits an experimental design well suited for overlap correction analyses. It likely provides enough data to avoid collinearity. It thus enabled the analysis of RT effects on neural responses with an approach recommended in recent literature that has not been implemented thus far.

The initial hypothesis that the P300 amplitude difference between conditions stems from an interaction of overlap and varying RTs was rejected for stimulus- and response-locked rERPs. The difference in P300 mean amplitude between target and distractor conditions can only be partially explained by overlap or an interaction of overlap and varying RTs.

The results indicate nonlinear RT effects on stimulus- and response-locked rERPs. The present study furthermore expands existing evidence that overlapping neural responses have a large effect on ERPs estimated via the traditional averaging approach (Dimigen & Ehinger, 2021; Ehinger & Dimigen, 2019; Smith & Kutas, 2015b). It, therefore, highlights the necessity to apply sophisticated data-analytic methods like deconvolution modelling for overlap correction in future studies if overlapping ERPs are present in the data. With this approach, the time course of neural responses can be resolved more accurately than with the traditional ERP averaging approach. True cognitive effects between conditions can be distinguished from spurious effects resulting from overlapping potentials, varying event durations, and other covariates influencing ERPs (non)linearly (Dimigen & Ehinger, 2021; Ehinger & Dimigen, 2019; Smith & Kutas, 2015b).

5 GERMAN SUMMARY

Ereigniskorrelierte Potenziale (EKPs) bieten eine hervorragende zeitliche Auflösung für die Isolierung neurokognitiver Prozesse. Neuronale Prozesse, die im Elektroenzephalogramm (EEG) aufgrund linearer Summation miteinander vermischt sind müssen unterschieden werden, um die Dynamiken von sensorischer Kodierung, Entscheidungsfindung und motorischen Befehlen, die das menschliche Verhalten bestimmen, zu untersuchen. ERPs überlappen aufgrund der engen zeitlichen Nähe benachbarter Ereignisse. Häufig variiert auch die Dauer von Ereignissen, z.B. aufgrund natürlicher Schwankungen der Reaktionszeit (RZ) oder experimenteller Variation der Präsentationsdauer von Stimuli. Überlappung neuronaler Prozesse und variierende Ereignisdauer stellen eine große methodische Herausforderung für die adäquate Isolierung von EKPs dar. In dieser Studie habe ich ein "Oddball"-Experiment durchgeführt und die Auswirkungen von Überlappungen und variierenden Ereignisdauern auf neuronale Prozesse analysiert. Die Implementierung des Deconvolution-Modells ermöglichte, Überlappung zu berücksichtigen und zeigte signifikante Effekte von Überlappung im Vergleich zum traditionellen Mittelwertbildungsansatz-Ansatz um EKPs zu berechnen. Das Hinzufügen der RZ als Prädiktor, modelliert durch Spline-Regression, offenbarte darüber hinaus, dass die natürliche Variation von RZ einen nichtlinearen Effekt auf EKP-Berechnungen hatte. Die Kontrolle von Überlappung und variierenden RZ führte zu einem signifikant geringeren Unterschied zwischen den neuronalen Prozessen der Verarbeitung der unterschiedlichen Versuchsbedingungen im Vergleich zum Mittelwertbildungsansatz-Ansatz. Daher führen Überlappung und unterschiedliche Ereignisdauern zu verzerrten Schätzungen und falschen Rückschlüssen auf die Dynamik neuronaler Prozesse, wenn sie nicht berücksichtigt werden. Dies unterstreicht, wie wichtig es ist, adäquate datenanalytische Methoden zur Analyse von EEG-Daten einzusetzen, um sinnvolle EKP-Berechnungen zu erhalten. Die mangelnde Übereinstimmung der hier erzielten Ergebnisse mit denen einer früheren Studie, von der das experimentelle Paradigma adaptiert wurde, erfordert eine weitere Analyse.

BIBLIOGRAPHY

REFERENCES

Amsel, B. D. (2011). Tracking real-time neural activation of conceptual knowledge using single-trial event-related potentials. *Neuropsychologia*, *49*(5), 970–983. https://doi.org/10.1016/j.neuropsychologia.2011.01.003

Bezanson, J., Edelman, A., Karpinski, S., & Shah, V. B. (2017). Julia: A fresh approach to numerical computing. *SIAM Review*, *59*(1), 65–98. https://doi.org/10.1137/141000671

Bhattacharyya, S., Konar, A., & Tibarewala, D. N. (2014). Motor imagery, P300 and error-related EEG-based robot arm movement control for rehabilitation purpose. *Medical & Biological Engineering & Computing*, *52*(12), 1007–1017. https://doi.org/10.1007/s11517-014-1204-4

Blinowska, K., & Durka, P. (2006). Electroencephalography (EEG). In *Wiley Encyclopedia of Biomedical Engineering*. John Wiley & Sons, Ltd. https://doi.org/10.1002/9780471740360.ebs0418

Brainard, D. H. (1997). The psychophysics toolbox. *Spatial Vision*, *10*(4), 433–436. https://doi.org/10.1163/156856897X00357

Cohen, J., & Polich, J. (1997). On the number of trials needed for P300. *International Journal of Psychophysiology*, *25*(3), 249–255. https://doi.org/10.1016/S0167-8760(96)00743-X

Dale, A. M., & Buckner, R. L. (1997). Selective averaging of rapidly presented individual trials using fMRI. *Human Brain Mapping*, *5*(5), 329–340. https://doi.org/10.1002/(SICI)1097-0193(1997)5:5<329::AID-HBM1>3.0.CO;2-5

Dandekar, S., Ding, J., Privitera, C., Carney, T., & Klein, S. A. (2012). The fixation and saccade P3. *PLOS ONE*, *7*(11), e48761. https://doi.org/10.1371/journal.pone.0048761

de Cheveigné, A. (2020). ZapLine: A simple and effective method to remove power line artifacts. *NeuroImage*, *207*, 116356. https://doi.org/10.1016/j.neuroimage.2019.116356

Di Russo, F., Lucci, G., Sulpizio, V., Berchicci, M., Spinelli, D., Pitzalis, S., & Galati, G. (2016). Spatiotemporal brain mapping during preparation, perception, and action. *NeuroImage*, *126*, 1–14. https://doi.org/10.1016/j.neuroimage.2015.11.036

Dimigen, O., & Ehinger, B. V. (2021). Regression-based analysis of combined EEG and eye-tracking data: Theory and applications. *Journal of Vision*, *21*(1), 3. https://doi.org/10.1167/jov.21.1.3

Donchin, E., & Coles, M. G. H. (1988). Is the P300 component a manifestation of context updating? *Behavioral and Brain Sciences*, *11*(3), 357–374. https://doi.org/10.1017/S0140525X00058027

Duncan-Johnson, C. C., & Donchin, E. (1977). On quantifying surprise: The variation of event-related potentials with subjective probability. *Psychophysiology*, *14*(5), 456–467. https://doi.org/10.1111/j.1469-8986.1977.tb01312.x

Ehinger, B. V., & Dimigen, O. (2019). Unfold: An integrated toolbox for overlap correction, non-linear modeling, and regression-based EEG analysis. *PeerJ*, *7*, e7838. https://doi.org/10.7717/peerj.7838

Farwell, L. A., & Donchin, E. (1988). Talking off the top of your head: Toward a mental prosthesis utilizing event-related brain potentials. *Electroencephalography and Clinical Neurophysiology*, *70*(6), 510–523. https://doi.org/10.1016/0013-4694(88)90149-6

Glickstein, M. (2000). How are visual areas of the brain connected to motor areas for the sensory guidance of movement? *Trends in Neurosciences*, *23*(12), 613–617. https://doi.org/10.1016/S0166-2236(00)01681-7

Gold, J. I., & Shadlen, M. N. (2007). The neural basis of decision making. *Annual Review of Neuroscience*, *30*(1), 535–574. https://doi.org/10.1146/annurev.neuro.29.051605.113038

Gramann, K., Ferris, D. P., Gwin, J., & Makeig, S. (2014). Imaging natural cognition in action. *International Journal of Psychophysiology*, *91*(1), 22–29. https://doi.org/10.1016/j.ijpsycho.2013.09.003

Gramfort, A., Luessi, M., Larson, E., Engemann, D., Strohmeier, D., Brodbeck, C., Goj, R., Jas, M., Brooks, T., Parkkonen, L., & Hämäläinen, M. (2013). MEG and EEG data analysis with MNE-Python. *Frontiers in Neuroscience*, *267*. https://www.frontiersin.org/articles/10.3389/fnins.2013.00267

Hansen, J. C. (1983). Separation of overlapping waveforms having known temporal distributions. *Journal of Neuroscience Methods*, *9*(2), 127–139. https://doi.org/10.1016/0165-0270(83)90126-7

Hauk, O., Davis, M. H., Ford, M., Pulvermüller, F., & Marslen-Wilson, W. D. (2006). The time course of visual word recognition as revealed by linear regression analysis of ERP data. *NeuroImage*, *30*(4), 1383–1400. https://doi.org/10.1016/j.neuroimage.2005.11.048

Hendrix, P., Bolger, P., & Baayen, H. (2017). Distinct ERP signatures of word frequency, phrase frequency, and prototypicality in speech production. *Journal of Experimental Psychology: Learning, Memory, and Cognition*, *43*, 128–149. https://doi.org/10.1037/a0040332

Hillyard, S. A., Squires, K. C., Bauer, J. W., & Lindsay, P. H. (1971). Evoked potential correlates of auditory signal detection. *Science*, *172*(3990), 1357–1360. https://doi.org/10.1126/science.172.3990.1357

Horváth, G., Nemes, V. A., Radó, J., Czigler, A., Török, B., Buzás, P., & Jandó, G. (2018). Simple reaction times to cyclopean stimuli reveal that the binocular system is tuned to react faster to near than to far objects. *PLOS ONE*, *13*(1), e0188895. https://doi.org/10.1371/journal.pone.0188895

Hsu, S.-H., Pion-Tonachini, L., Palmer, J., Miyakoshi, M., Makeig, S., & Jung, T.-P. (2018). Modeling brain dynamic state changes with adaptive mixture independent component analysis. *NeuroImage*, *183*, 47–61. https://doi.org/10.1016/j.neuroimage.2018.08.001

Huster, R. J., Enriquez-Geppert, S., Lavallee, C. F., Falkenstein, M., & Herrmann, C. S. (2013). Electroencephalography of response inhibition tasks: Functional networks and cognitive contributions. *International Journal of Psychophysiology*, *87*(3), 217–233. https://doi.org/10.1016/j.ijpsycho.2012.08.001

Hutmacher, F. (2019). Why is there so much more research on vision than on any other sensory modality? *Frontiers in Psychology*, *10*, 2246. https://doi.org/10.3389/fpsyg.2019.02246

Jung, T.-P., Makeig, S., Westerfield, M., Townsend, J., Courchesne, E., & Sejnowski, T. J. (2001). Analysis and visualization of single-trial event-related potentials. *Human Brain Mapping*, *14*(3), 166–185. https://doi.org/10.1002/hbm.1050

Kappenman, E. S., Farrens, J. L., Zhang, W., Stewart, A. X., & Luck, S. J. (2021a). ERP CORE: An open resource for human event-related potential research. *NeuroImage*, *225*. https://doi.org/10.1016/j.neuroimage.2020.117465

Kappenman, E. S., Farrens, J. L., Zhang, W., Stewart, A. X., & Luck, S. J. (2021b). Supplementary materials for ERP CORE: An open resource for human event-related potential research. *NeuroImage*, *225*. https://doi.org/10.1016/j.neuroimage.2020.117465

Karniski, W., & Clifford Blair, R. (1989). Topographical and temporal stability of the P300. *Electroencephalography and Clinical Neurophysiology*, *72*(5), 373–383. https://doi.org/10.1016/0013-4694(89)90043-6

Kelly, S. P., & O'Connell, R. G. (2013). Internal and external influences on the rate of sensory evidence accumulation in the human brain. *Journal of Neuroscience*, *33*(50), 19434–19441. https://doi.org/10.1523/JNEUROSCI.3355-13.2013

Kelly, S. P., & O'Connell, R. G. (2015). The neural processes underlying perceptual decision making in humans: Recent progress and future directions. *Journal of Physiology-Paris*, *109*(1), 27–37. https://doi.org/10.1016/j.jphysparis.2014.08.003

Kleiner, M., Brainard, D. H., & Pelli, D. (2007). What's new in psychtoolbox-3?

Klug, M., & Kloosterman, N. A. (2022). Zapline-plus: A Zapline extension for automatic and adaptive removal of frequency-specific noise artifacts in M/EEG. *Human Brain Mapping*, *43*(9), 2743–2758. https://doi.org/10.1002/hbm.25832

Kok, A. (2001). On the utility of P3 amplitude as a measure of processing capacity. *Psychophysiology*, *38*(3), 557–577. https://doi.org/10.1017/S0048577201990559

Kryuchkova, T., Tucker, B. V., Wurm, L. H., & Baayen, R. H. (2012). Danger and usefulness are detected early in auditory lexical processing: Evidence from electroencephalography. *Brain and Language*, *122*(2), 81–91. https://doi.org/10.1016/j.bandl.2012.05.005

Kutas, M., McCarthy, G., & Donchin, E. (1977). Augmenting mental chronometry: The P300 as a measure of stimulus evaluation time. *Science*, *197*(4305), 792–795. https://doi.org/10.1126/science.887923

Lammers, W. J., & Badia, P. (1989). Habituation of P300 to target stimuli. *Physiology & Behavior*, *45*(3), 595–601. https://doi.org/10.1016/0031-9384(89)90079-6

Liebherr, M., Corcoran, A. W., Alday, P. M., Coussens, S., Bellan, V., Howlett, C. A., Immink, M. A., Kohler, M., Schlesewsky, M., & Bornkessel-Schlesewsky, I. (2021). EEG and behavioral correlates of attentional processing while walking and navigating naturalistic environments. https://doi.org/10.1038/s41598-021-01772-8

Litvak, V., Jha, A., Flandin, G., & Friston, K. (2013). Convolution models for induced electromagnetic responses. *NeuroImage*, *64*, 388–398. https://doi.org/10.1016/j.neuroimage.2012.09.014

Luck, S. J. (2014). *An introduction to the event-related potential technique* (Second edition). The MIT Press.

Lütkenhöner, B. (2010). Baseline correction of overlapping event-related responses using a linear deconvolution technique. *NeuroImage*, *52*(1), 86–96. https://doi.org/10.1016/j.neuroimage.2010.03.053

Michalewski, H. J., Prasher, D. K., & Starr, A. (1986). Latency variability and temporal interrelationships of the auditory event-related potentials (N1, P2, N2, and P3) in normal subjects. *Electroencephalography and Clinical Neurophysiology/Evoked Potentials Section*, *65*(1), 59–71. https://doi.org/10.1016/0168-5597(86)90037-7

Mullen, T. R., Kothe, C. A. E., Chi, Y. M., Ojeda, A., Kerth, T., Makeig, S., Jung, T.-P., & Cauwenberghs, G. (2015). Real-time neuroimaging and cognitive monitoring using wearable dry EEG. *IEEE Transactions on Biomedical Engineering*, *62*(11), 2553–2567. https://doi.org/10.1109/TBME.2015.2481482

Murray, J. G., Ouyang, G., & Donaldson, D. I. (2019). Compensation of trial-to-trial latency jitter reveals the parietal retrieval success effect to be both variable and thresholded in older adults. *Frontiers in Aging Neuroscience*, *11*, 179. https://doi.org/10.3389/fnagi.2019.00179

Negi, S., & Mitra, R. (2020). Fixation duration and the learning process: An eye tracking study with subtitled videos. *Journal of Eye Movement Research*, *13*(6), 10.16910/jemr.13.6.1. https://doi.org/10.16910/jemr.13.6.1

O'Connell, R. G., Dockree, P. M., & Kelly, S. P. (2012). A supramodal accumulation-to-bound signal that determines perceptual decisions in humans. *Nature Neuroscience*, *15*(12), Article 12. https://doi.org/10.1038/nn.3248

Ouyang, G., Herzmann, G., Zhou, C., & Sommer, W. (2011). Residue iteration decomposition (RIDE): A new method to separate ERP components on the basis of latency variability in single trials. *Psychophysiology*, *48*(12), 1631–1647. https://doi.org/10.1111/j.1469-8986.2011.01269.x

Ouyang, G., Sommer, W., & Zhou, C. (2015). A toolbox for residue iteration decomposition (RIDE)—A method for the decomposition, reconstruction, and single trial analysis of event related potentials. *Journal of Neuroscience Methods*, *250*, 7–21. https://doi.org/10.1016/j.jneumeth.2014.10.009

Pernet, C. R., Martinez-Cancino, R., Truong, D., Makeig, S., & Delorme, A. (2021). From BIDS-formatted EEG data to sensor-space group results: A fully reproducible workflow with EEGLAB and LIMO EEG. *Frontiers in Neuroscience*, *14*. https://www.frontiersin.org/articles/10.3389/fnins.2020.610388

Pion-Tonachini, L., Kreutz-Delgado, K., & Makeig, S. (2019). ICLabel: An automated electroencephalographic independent component classifier, dataset, and website. *NeuroImage*, *198*, 181–197. https://doi.org/10.1016/j.neuroimage.2019.05.026

Polich, J. (2007). Updating P300: An integrative theory of P3a and P3b. *Clinical Neurophysiology*, *118*(10), 2128–2148. https://doi.org/10.1016/j.clinph.2007.04.019

Raggi, A., Lanza, G., & Ferri, R. (2021). A review on P300 in obsessive-compulsive disorder. *Frontiers in Psychiatry*, *12*. https://www.frontiersin.org/articles/10.3389/fpsyt.2021.751215

Rakshit, A., Konar, A., & Nagar, A. K. (2020). A hybrid brain-computer interface for closed-loop position control of a robot arm. *IEEE/CAA Journal of Automatica Sinica*, *7*(5), 1344–1360. https://doi.org/10.1109/JAS.2020.1003336

Rossini, P. M., Rossi, S., Babiloni, C., & Polich, J. (2007). Clinical neurophysiology of aging brain: From normal aging to neurodegeneration. *Progress in Neurobiology*, *83*(6), 375–400. https://doi.org/10.1016/j.pneurobio.2007.07.010

Rossion, B., & Jacques, C. (2008). Does physical interstimulus variance account for early electrophysiological face sensitive responses in the human brain? Ten lessons on the N170. *NeuroImage*, *39*(4), 1959–1979. https://doi.org/10.1016/j.neuroimage.2007.10.011

Rousselet, G. A., Husk, J. S., Pernet, C. R., Gaspar, C. M., Bennett, P. J., & Sekuler, A. B. (2009). Age-related delay in information accrual for faces: Evidence from a parametric, single-trial EEG approach. *BMC Neuroscience*, *10*(1), 114. https://doi.org/10.1186/1471-2202-10-114

Rousselet, G. A., Pernet, C. R., Bennett, P. J., & Sekuler, A. B. (2008). Parametric study of EEG sensitivity to phase noise during face processing. *BMC Neuroscience*, *9*(1), 98. https://doi.org/10.1186/1471-2202-9-98

Santosh, P. J., Malhotra, S., Raghunathan, M., & Mehra, Y. N. (1994). A study of P300 in melancholic depression—Correlation with psychotic features. *Biological Psychiatry*, *35*(7), 474–479. https://doi.org/10.1016/0006-3223(94)90046-9

Sassenhagen, J. (2019). How to analyse electrophysiological responses to naturalistic language with time-resolved multiple regression. *Language, Cognition and Neuroscience*, *34*(4), 474–490. https://doi.org/10.1080/23273798.2018.1502458

Sellers, E. W., Arbel, Y., & Donchin, E. (2012). BCIs that use P300 event-related potentials. In *Brain–Computer Interfaces: Principles and Practice*. Oxford University Press. https://doi.org/10.1093/acprof:oso/9780195388855.003.0012

Smith, N. J., & Kutas, M. (2015a). Regression-based estimation of ERP waveforms: I. The rERP framework. *Psychophysiology*, *52*(2), 157–168. https://doi.org/10.1111/psyp.12317

Smith, N. J., & Kutas, M. (2015b). Regression-based estimation of ERP waveforms: II. Nonlinear effects, overlap correction, and practical considerations. *Psychophysiology*, *52*(2), 169–181. https://doi.org/10.1111/psyp.12320

Squires, K. C., Hillyard, S. A., & Lindsay, P. H. (1973). Vertex potentials evoked during auditory signal detection: Relation to decision criteria. *Perception & Psychophysics*, *14*(2), 265–272. https://doi.org/10.3758/BF03212388

Sutton, S., Braren, M., Zubin, J., & John, E. R. (1965). Evoked-potential correlates of stimulus uncertainty. *Science*, *150*(3700), 1187–1188. https://doi.org/10.1126/science.150.3700.1187

Tanskanen, T., Näsänen, R., Ojanpää, H., & Hari, R. (2007). Face recognition and cortical responses: Effect of stimulus duration. *NeuroImage*, *35*(4), 1636–1644. https://doi.org/10.1016/j.neuroimage.2007.01.023

Tremblay, A., & Newman, A. J. (2015). Modeling nonlinear relationships in ERP data using mixed-effects regression with R examples. *Psychophysiology*, *52*(1), 124–139. https://doi.org/10.1111/psyp.12299

Twomey, D. M., Murphy, P. R., Kelly, S. P., & O'Connell, R. G. (2015). The classic P300 encodes a build-to-threshold decision variable. *European Journal of Neuroscience*, *42*(1), 1636–1643. https://doi.org/10.1111/ejn.12936

Völker, M., Fiederer, L. D. J., Berberich, S., Hammer, J., Behncke, J., Kršek, P., Tomášek, M., Marusič, P., Reinacher, P. C., Coenen, V. A., Helias, M., Schulze-Bonhage, A., Burgard, W., & Ball, T. (2018). The dynamics of error processing in the human brain as reflected by high-gamma activity in noninvasive and intracranial EEG. *NeuroImage*, *173*, 564–579. https://doi.org/10.1016/j.neuroimage.2018.01.059

Wilkinson, G. N., & Rogers, C. E. (1973). Symbolic description of factorial models for analysis of variance. *Journal of the Royal Statistical Society. Series C (Applied Statistics)*, *22*(3), 392–399. https://doi.org/10.2307/2346786

Woldorff, M. G. (1993). Distortion of ERP averages due to overlap from temporally adjacent ERPs: Analysis and correction. *Psychophysiology*, *30*(1), 98–119. https://doi.org/10.1111/j.1469-8986.1993.tb03209.x

Wood, S. N. (2017). *Generalized additive models: An introduction with R* (2nd ed.). CRC Press.

LIST OF FIGURES

LIST OF TABLES

ERKLÄRUNG

Hiermit versichere ich, dass die Arbeit

Investigating the effects of overlap and event durations on neural responses

von mir selbst und ohne jede unerlaubte Hilfe angefertigt wurde. Die Stellen der Arbeit einschließlich der Tabellen und Abbildungen, die anderen Werken dem Wortlaut oder dem Sinn nach entnommen sind, habe ich in jedem einzelnen Fall kenntlich gemacht und die Herkunft nachgewiesen. Die Arbeit hat weder vollständig noch in wesentlichen Teilen einer anderen Stelle zur Prüfung vorgelegen. Die Arbeit wurde weder vollständig noch in Teilen bereits veröffentlicht. Das elektronische Exemplar stimmt mit den anderen Exemplaren überein.

.....

Ort, Datum und Unterschrift